Biophysical Chemistry 280 (2022) 106701

Contents lists available at ScienceDirect

Biophysical Chemistry

journal homepage: www.elsevier.com/locate/biophyschem

Potential allosteric sites captured in glycolytic enzymes via residue-based network models: Phosphofructokinase, glyceraldehyde-3-phosphate dehydrogenase and pyruvate kinase

Metehan Celebi [a], Tugce Inan [b], Ozge Kurkcuoglu [b], Ebru Demet Akten [c,*]

[a] Graduate Program of Computational Biology and Bioinformatics, Graduate School of Science and Engineering, Kadir Has University, Istanbul, Turkey
[b] Department of Chemical Engineering, Istanbul Technical University, Istanbul, Turkey
[c] Department of Bioinformatics and Genetics, Faculty of Engineering and Natural Sciences, Kadir Has University, Istanbul, Turkey

ARTICLE INFO

Keywords:
Allostery
Glycolytic
Residue network model
Hub residues
Low-frequency normal mode
Communication pathway

ABSTRACT

Likelihood of new allosteric sites for glycolytic enzymes, phosphofructokinase (PFK), glyceraldehyde-3-phosphate dehydrogenase (GADPH) and pyruvate kinase (PK) was evaluated for bacterial, parasitic and human species. Allosteric effect of a ligand binding at a site was revealed on the basis of low-frequency normal modes via C_α-harmonic residue network model. In bacterial PFK, perturbation of the proposed allosteric site outperformed the known allosteric one, producing a high amount of stabilization or reduced dynamics, on all catalytic regions. Another proposed allosteric spot at the dimer interface in parasitic PFK exhibited major stabilization effect on catalytic regions. In parasitic GADPH, the most desired allosteric response was observed upon perturbation of its tunnel region which incorporated key residues for functional regulation. Proposed allosteric site in bacterial PK produced a satisfactory allosteric response on all catalytic regions, whereas in human and parasitic PKs, a partial inhibition was observed. Residue network model based solely on contact topology identified the 'hub residues' with high betweenness tracing plausible allosteric communication pathways between distant functional sites. For both bacterial PFK and PK, proposed sites accommodated hub residues twice as much as the known allosteric site. Tunnel region in parasitic GADPH with the strongest allosteric effect among species, incorporated the highest number of hub residues. These results clearly suggest a one-to-one correspondence between the degree of allosteric effect and the number of hub residues in that perturbation site, which increases the likelihood of its allosteric nature.

1. Introduction

Allosteric communication between two distant sites is a key feature of many enzymes catalyzing a wide range of biochemical reactions in living systems. It is widely accepted as an intrinsic property that was evolutionarily optimized to regulate the enzymatic activity [1,2]. It consists of a bound ligand that induces a conformational change at the interaction site, which then propagates to a distant site. This site is usually the catalytic region where the affinity of the enzyme towards its substrate either increases or decreases. This "revolutionized" model allows a rapid transition between two conformational minima. An alternative definition of allostery is based on the notion that proteins are dynamic ensembles of conformational states. It is the ligand-binding that triggers the re-distribution or shuffling of that ensemble such that an altered conformation at a distant site will be more or less suitable for a substrate binding. This dynamic convertibility, which allows the protein to be at different functional states, is now widely accepted as an intrinsic property of all proteins encoded in their three-dimensional structures.

Nearly five decades ago, two plausible models were proposed for allostery. They are the well-known concerted MWC model [3] where the oligomeric protein interconverts between two distinct conformations (tense and relaxed), and the sequential KNF model [4] where monomeric units change conformations, one at a time. However, both models associated allostery to multi-chain proteins only. In contrast, current models associate allostery to a wide range of proteins, even to those assumed to be non-allosteric [5,6]. Several studies showed that one can create an allosteric protein from non-allosteric ones, when a

* Corresponding author.
E-mail address: demet.akten@khas.edu.tr (E.D. Akten).

https://doi.org/10.1016/j.bpc.2021.106701
Received 8 September 2021; Received in revised form 12 October 2021; Accepted 19 October 2021
Available online 30 October 2021

perturbation such as a strong binder or a mutation was introduced, simply by shifting the population of the ensemble, which will either favor or disfavor the binding of certain substrates [7–9]. Reverse perturbation model introduced by Tee and his coworkers can identify latent allosteric sites as a result of a perturbation applied to functional sites. As functional and allosteric sites are dynamically coupled, one can use this method for inducing and tuning allosteric communication [10]. Moreover, allostery can be effectively used in drug design studies to create a drug molecule that would be highly specific for a particular species as allosteric sites are more prone to mutations than active sites [11,12].

For computational drug design, the first step is to identify allosteric binding sites that would induce the desired effect on the functional site. There exist several structure-based methodologies, which are based on normal mode analysis using elastic network models or Molecular Dynamics (MD) simulations [13–15]. The change in the cooperative fluctuations, which describe the receptor's global motion as a result of a bound ligand can be monitored. The whole surface of the receptor can be also scanned for potential allosteric sites, which show the largest variations in the low-frequency normal modes [16]. Mutation, which is another type of structural perturbation, was extensively studied via MD simulations to demonstrate the large-scale conformational variations between wild-type and mutant forms [17]. In addition to the highly correlated, low-frequency normal mode vibrations, the perturbation effect can manifest itself in the form of uncorrelated random local anharmonic motions of individual atoms or groups [18]. Monitoring the changes in frequencies and amplitudes of thermal fluctuations about the mean conformational state conform to the general model introduced by Cooper and Dryden [19] which describes allosteric communication between distinct binding sites in the absence of a conformational change. All these changes in the dynamic fluctuations around the mean reflect the entropic side of allostery.

A more complete account of the allosteric communication would incorporate enthalpic components alongside entropy. The enthalpic constituent is reflected by a more classical view which tends to explain allostery in terms of structural variations [18,20,21]. A modification at one site simply propagates from one residue to another through a series of conformational changes that will assist in minimizing the overall enthalpic energy and consequently the system will reach the thermodynamic equilibrium. This so-called conformational spread explains the machinery of many proteins such as ion pumps, signaling proteins, viral fusion proteins, chaperonins, and many more [22,23]. Similar to protein folding, there exist multiple pathways for transmitting the conformational change from one site to another distant site. One of those defined pathways will be more favorable than the others. It is also argued that these communication pathways already exist in the repertoire of the protein dynamics [24]. In other words, information is transmitted through an evolutionarily conserved network of residues with high statistical frequencies. It is analogous to a functional allosteric circuit or a "hot wire" that guarantees site-to-site communication [25]. Over the years, graph theoretical (network theory) methods have been widely used in establishing this circuit and determining its constitutive residues [26,27]. The protein was represented as a network of interacting nodes located usually at backbone C_α atoms connected by links if separated by less than a physically acceptable cut-off distance. For a given network, the importance of a node was usually assessed using centrality measures such as betweenness, closeness, and degree [28]. An alternative approach developed by del Sol and his coworkers [29] identified nodes (or residues) that disrupted the interconnectedness the most when removed from the network, which in turn manifested with a significant increase in the characteristic path length. These centrally conserved residues were further identified as mediators of the signaling process in different protein families as confirmed by experiments [30].

Recent advances in computational tools predicting allosteric regions paved the way for allosteric drugs [31–33] which offer high specificity/selectivity in comparison to orthosteric drugs due to high degree of sequence variation among species observed at these allosteric sites. Especially, in the fight with pathogens, proteins functioning in the most critical biochemical pathways such as glycolysis were used as species-specific drug targets. Glycolysis in the cell converts glucose to pyruvate producing ATP and the glycolytic enzymes catalyzing all ten reactions of this pathway are common to both humans and pathogens. In this study, we investigated three of those enzymes, namely phosphofructokinase, glyceraldehyde-3-phosphate dehydrogenase and pyruvate kinase for which previously proposed allosteric sites [34] presented a high degree of sequence variation between bacterial/parasitic and human species. In our current work, all proposed allosteric sites were re-evaluated using a structure-based statistical mechanical model of allostery (SBSMMA) via the interface AlloSigMA [35–37], which quantifies the effect of perturbation caused by a ligand binding at the potential allosteric site on rest of the protein. Ligand binding was mimicked via an increase in the interaction strength of contacts between residues at the binding site and its effect was measured via an allosteric potential described in terms of a linear combination of normal modes. In the second part, the residue network model with the betweenness centrality measure was employed to further assess the likelihood of these sites to possess allosteric properties. The network model was based on the contact topology of the intact protein which was described as a network of nodes linked by edges. The nodes were placed at C_α atoms and the lengths of the edges were assigned such that the bias towards covalent bonds was removed and tertiary interactions were favoured. The betweenness centrality measure of the resulting network revealed the hot-wires that accommodated residues linking distant functional sites, as was previously shown for the bacterial ribosome [38].

The systems under study were three glycolytic enzymes belonging to human, bacterial (*S.aureus*) and parasitic (*T.brucei*, *T.cruzei*, and *L. mexicana*) species. Two of these enzymes were the well-studied allosteric enzymes, phosphofructokinase, and pyruvate kinase. Glyceraldehyde-3-phosphate dehydrogenase was the third enzyme studied, which had no reported allosteric property so far. The two approaches employed in this study incorporated distinct models to approximate the interaction energies between neighboring residues, i.e. harmonic functional motions and native contacts of crystal structures, yet they had a high agreement on the potential allosteric sites of the studied enzymes, which can be further tested using docking studies and in vitro assays to develop species-specific therapeutics.

2. Methods

2.1. System preparation

X-ray crystallographic structures of all three glycolytic enzymes, phosphofructokinase (PFK) [39–43], glyceraldehyde-3-phosphate dehydrogenase (GADPH) [44–50], and pyruvate kinase (PK) [51–59] belonging to different species were extracted from the Protein Data Bank

Table 1
X-ray crystallographic structures of three glycolytic enzymes used in AlloSigMA evaluations and betweenness calculations.

Enzyme	Bacterium (*S.aureus*)	Parasite PFK *(T.brucei)*, GADPH *(T.cruzi)*, PK *(L.mexicana)*	Human (*H.sapiens*)
PFK	5xza†, 5xoe‡, 5xz6‡, 5xz7†, 5xz8‡, 5xz9‡	3f5m†, 2hig‡, 6qu5‡	4rh3§, 4u1r‡, 4wl0‡, 4xz2‡
GADPH	3hq4†, 3k9q‡, 3k73‡, 3l6o‡, 3lc2‡, 3lvf‡	3dmt§, 1k3t‡, 1ml3‡, 1qxs‡, 3ids‡	1znq‡, 4wnc‡, 4wni‡, 6iq6‡
PK	3t0t†, 3t05‡, 3t07‡	1pkl†, 3e0v‡, 3hqp‡, 3hqq‡	4g1n§, 1t5a‡, 3gqy‡, 4fxf‡, 6gg5‡, 6gg6‡

† Used in both AlloSigMA and betweenness calculations.
‡ Only used in betweenness calculations.
§ Only used in AlloSigMA calculations.

with the corresponding IDs as listed in Table 1. Different parasitic species were studied for each enzyme, *T.brucei* for PFK, *T.cruzi* for GAPDH, and *L.mexicana* for PK, whereas the same bacterial species *S.aureus* was used in all three cases. As indicated with different labels in Table 1, only one version of the structure was used for AlloSigMA, whereas multiple X-ray structures were employed for betweenness calculations with the residue network model.

2.2. Perturbation sites used in AlloSigMA[35–37] and calculation of mean free energy of binding, ΔG

Several druggable binding sites were identified in our previous analysis by Ayyildiz and coworkers [34] for each species of all three enzymes cited in Table 1. First, computational solvent-mapping via FTMap tool [60] was used to identify all possible ligand binding sites via docking small drug-like organic compounds (or solvent) over the entire receptor. A total of 2000 poses generated for each probe were energy-minimized and clustered based on proximity. Clusters were then ranked by their Boltzmann-averaged energy values. Overlapping clusters of different solvent types were assembled into consensus sites identified as "hot spots". Then, a residue scanning method based on a coarse-grained elastic network model (ENM) [16] was employed to determine the percentage frequency shift for each residue which is defined as the change in the collective mode's eigenvalues upon adding extra nodes (side chain heavy atoms) to the selected residue represented by its α-Carbon only. Finally, FTMap and ENM-based residue scanning results were merged by determining a mean percentage frequency shift value which represents the average over all n residues neighboring all the bound solvent molecules in that cluster. A cluster with a mean value less than 50% was simply discarded from analysis as its interaction with a ligand would have a negligible impact on the global dynamics of the receptor. Regions which incorporated residues with highest frequency shift were simply proposed as potential allosteric sites [61].

The overall effect of the perturbation imposed on the proposed allosteric sites was evaluated by taking the average of per-residue free energy changes (ΔG) over all residues belonging to the catalytic (functional) sites. ΔG quantifies the maximal configurational work that is exerted on a residue as a result of a bound ligand at a distant site and depends on the number of low frequency normal modes [34]. Accordingly, a positive ΔG indicated an increase in dynamics whereas a negative ΔG shows reduced dynamics or stabilization. The overall effect of the perturbation imposed on the proposed sites was evaluated by taking the average of ΔG values over all residues belonging to the catalytic (functional) sites. A desirable outcome of an allosterically inhibiting site would be a negative mean ΔG for the majority of catalytic regions. As listed in Table 2, additional trial runs were conducted on the known allosteric sites of two bacterial enzymes PFK and PK reported in the literature [50,62] to make a direct comparison with the results of the proposed allosteric site.

2.3. Residue network model and betweenness centrality calculations

The protein's native structure was described as a weighted bi-directional graph of nodes linked by edges. The nodes were placed at C_α atoms. The local interaction strength a_{ij} between two residues i and j was calculated based on their heavy atom-pairs within a cutoff distance of 4.5 Å as in previous studies [63,64] using,

$$a_{ij} = \frac{N_{ij}}{\sqrt{N_i N_j}} \quad (1)$$

where N_{ij} is the total number of atom-atom contacts, and N_i and N_j are the numbers of heavy atoms in i^{th} and j^{th} residues, respectively. Then, the inverse of the local interaction strength, i.e. $1/a_{ij}$, was assigned as the length of the edge connecting the (i,j) node pairs. With this model, the bias towards the covalent bonds was removed and tertiary interactions

Table 2
Selected residues at the perturbation sites in PFK, GADPH and PK for AlloSigMA evaluations.

Enzyme	Species	Trial Runs	Binding Sites[†] (Chain ID: Residue IDs)
PFK	*S.aureus (5xz7[‡])*	#1 Proposed Site (Top Druggable)	**A**:N130,D136-T143,L145,N146, W181,T259-D262,V264-A266,R268, I288-N291 **B**:F137-T143,L145,N146,W181, T259-D262,V264-A266,R268,I288, N291 **C**:N130,F137-T143,L145,N146, W181,T259,G260-D262,V264,A266, R268,I288,N291 **D**:N130,F137-T143,W181,T259-D262,V264-A266,R268,I288, N290, N291
		#2 Known Allosteric Site [54]	**A/B/C/D:** R21,R25,D59,R156,V186-E189,K215,I322
	T.brucei (3f5m[‡])	#1 Proposed Site (Top Druggable)	**A**:L84,A85,R237,Q242,N390,L393, C395,T397,L398,L401,M417,N420-Y422 **B**:R8-S11,N230,H236-T238,F241, Q242,Q282,V285,R435,L437,Q442, L443,Q446 **C**:L84-A86,D237,T390,L393,L401, N420-I423 **D**:L8-S11,N230,H236,T238,F241, Q242,F278,Q282,S432,R435,Q442, L443
		#5 Proposed Site	**A**:K247,Y375-I382 **B**:K247,Q250,A254,Y375-P378, Y380,M381 **C**:Y375-M381 **D**:Q250,Y375-I382
	H.Sapiens (4rh3[‡])	Proposed Site (Top Druggable)	**A/D**:M183,T187,D188,L191,Y223, V227,S315,F317,N390,F548,D553, P680-G686, K688,I722,V727 **B/C**:D182,M183,A316-D318,I320-A322,R324,L347-H351,N541,F548-D553,L556, N557, Y589,M593,S679, F681,D682,F685,I722-N726,W750
	S.aureus (3hq4[‡])	Proposed Site	**A**:D48-R53,Y180,A203-N205,P236-A238 **B**:D48-M50,A203-N205,P236,T239, S281,D282,V284 **C**:A203,E204,P236 **D**:D48-G52,A203,E204,P236,S281-V284
GADPH	*T.cruzi (3dmt[‡])*	Proposed Site	**A**:T54,V55,S195,Y196,A218-I221, P251-V255,S298-I302 **B/D**:T54-H56,S195,Y196,A218-I221,P251-S256,S298,A299,I302 **C**:T54,V55,S195,Y196,A218-I221, P251-V255,S298,A299,I302
	H.Sapiens (4wni[‡])	Proposed Site (Top Druggable)	**A**:T52,H53,A180,K181,L203-I206, P236-V240,S283-N287 **B**:S51,T52,A180,N204-I206,P236-V240,S283-N287 **C**:T52,A180,K181,L203-I206,P236-V240,S283-N287 **D**:S51,T52,A180,K181,L203-I206, P236-V240,S283-N287
PK	*S.aureus (3t0t[‡])*	#1 Proposed Site (Top Druggable)	**A**:K260,R264,N267,N299,Y302-G304,A337-Y340,K342,L343,D346, R347 **B**:K260,N299,Y302,D303,A337-Y340,K342,L343,D346 **C**:K260,R264,N267,N299,Y302, D303,D346,R347 **D**:Y302,Q338-Y340,K342,L343
		#2 Known Allosteric Site [45]	**A/C**:T353,A358,I361,S362,H365, T366,N369 **B**:T353,A358,I361,S362,H365,T366, N369,L370

(*continued on next page*)

Table 2 (*continued*)

Enzyme	Species	Trial Runs	Binding Sites† (Chain ID: Residue IDs)
		#3 Proposed Site	**D**:A358,I361,S362,H365,T366, N369,L370 **A**:K271,E324 **B**:G481,G483,R484,A572-Q574
	L. mexicana (1pkl‡)	Proposed Site (Top Druggable)	**C**:R19,R22,I23,L40-S46,V76-I78, C420,T427-T434,V437-S439
	H.Sapiens (4glm‡)	Proposed Site (Top Druggable)	**A**:F26,L27,H29,M30,L33,K311, C326,N350,V352-G355,A388-H391, Q393-F395,E397 **B**:F26,L27,M30,K311,N350,L353, D354,A388-L394,E397

† Proposed site residues are taken from Ayyildiz et al.[34]
‡ PDB ids extracted from PDB databank.

between residues were taken into account. Furthermore, the betweenness of the i^{th} node $C_B(i)$ was calculated as,

$$C_B(i) = \sum_{i \neq j \neq l} \frac{\sigma_{lj}(i)}{\sigma_{lj}} \quad (2)$$

Here, σ_{lj} is the number of shortest paths between l^{th} and j^{th} nodes and $\sigma_{lj}(i)$ is the number of shortest paths between l^{th} and j^{th} nodes intersecting the i^{th} node. C_B values were calculated for all the nodes forming the network, and a power-law distribution was observed for their frequencies. Accordingly, nodes with C_B values in the top 5% were considered as hub residues forming the hot-wires of the network and maintaining the site-to-site allosteric communication.

3. Results and discussion

3.1. The proposed allosteric site in S. aureus PFK outperformed the known allosteric site in restricting the dynamics of the catalytic region

Two distinct sites were used for perturbation in order to investigate the allosteric effect of ligand binding on the catalytic regions of PFK enzyme. As highlighted with dark blue surfaces on the top row of Fig. 1 (Run #1), the first binding (or perturbation) location was identified as the top druggable site proposed in our previous work by Ayyildiz and coworkers [34]. Due to the symmetric nature of the homotetramer, it incorporated two symmetric faces at the intersection of chains A/B and C/D. The second binding location presented on the right section (Run #2) of Fig. 1 was the well-reported allosteric site occupied by the inhibitor phosphoenol-pyruvate (PEP), which was retrieved from the PDB structure of 6pfk [59]. Similarly, it had symmetric counterparts on all four chains of the homotetramer structure (See Table S1 for the list of residues). Upon ligand binding, the allosteric effect was measured by the amount of change in the free energy, ΔG, for each residue. A colour gradient was used to bring out the regions displaying a decrease (blue), an increase (red) or no effect (white) on local dynamics. The increase in ΔG indicated a destabilization of that residue while a decrease indicated the opposite.

A mean allosteric free energy was determined for residues residing in each catalytic site occupied by the substrate F6P and ATP in addition to a complete profile of ΔG for each residue (See Fig. 1). Accordingly, the allosteric effect of the proposed site caused a decrease in mean ΔG (varying from −0.18 down to −0.78 kcal/mol) in F6P and ATP binding sites on all four chains. This was easily recognizable compared to the known allosteric site, which manifested a distinctly low positive mean ΔG values (0.04, 0.05 kcal/mol) signifying an almost null effect. Also, the main distinction between two trial runs was the degree of stabilization at the perturbation site, which created its unique ΔG profile. Upon perturbation (or restriction), the degree of stabilization observed at the proposed allosteric site was considerably higher than that

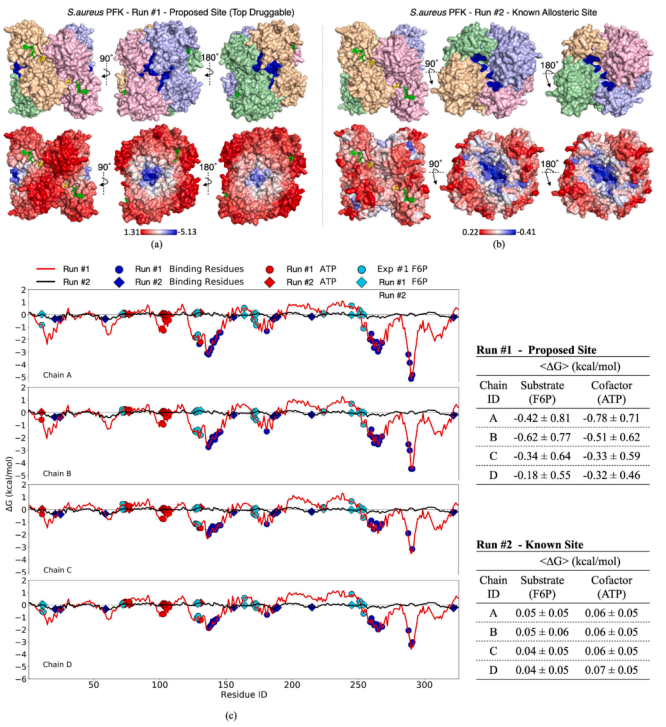

Fig. 1. AlloSigMA results for *S. aureus* PFK. Restrained residues colored in dark blue regions in (a) Run #1 (proposed allosteric site) and (b) Run #2 (known allosteric site). (c) full ΔG profile with corresponding mean ΔG values at the substrate F6P and cofactor ATP binding site. In (a) and (b) ATP and F6P represented in green and yellow sticks, respectively. First Row: PFK colored by chain (chain A: wheat, chain B: pale green, chain C: light blue, chain D: light pink). See Suppl Table 1 for corresponding residue IDs. Second Row: PFK colored based on ΔG values of each residue. Maximum and minimum values indicated on the spectrum bar below. (For interpretation of the references to colour in this figure legend, the reader is referred to the web version of this article.)

observed at the known allosteric site (−5.13 vs −0.41 kcal/mol). Also, ΔG profiles of two runs were clearly distinguishable: the known allosteric site displayed minor fluctuations in ΔG around zero whereas the proposed site's perturbation markedly disrupted the dynamics throughout the structure as indicated with red curves covering a wide range of negative values.

3.2. T. brucei PFK presented a potential allosteric site at the central interface connecting the two catalytic regions

Interestingly, the proposed site in *S. aureus* PFK had a correspondence at the same location in PFK belonging to species *T. brucei*. However, the perturbation of this site did cause an opposite effect on all four catalytic regions, which became destabilized in consequence. The increased dynamics was depicted in Fig. 2 by positive ΔG values (0.08–0.63 kcal/mol) under Run #1. This indicated an allosteric effect, which would potentially activate the catalytic regions instead of inhibiting. In addition, three more druggable sites proposed in our last analysis by Ayyildiz et al.[34] were targeted for *T. brucei* PFK, yet none induced the desired allosteric effect (See Table S1). The fourth evaluation covered a wide area connecting the two catalytic regions, yet the perturbation site was considered as proximate as it was within reach to catalytic sites. The last trial (Run #5) was a slight modification of the fourth: the perturbation was reduced to a confined region towards the midpoint, which became sufficiently cut off from the catalytic regions (8–9 Å away) to be considered allosteric.

Among the five evaluations, run #5 outperformed the other four, exhibiting a major allosteric effect on almost all four catalytic regions.

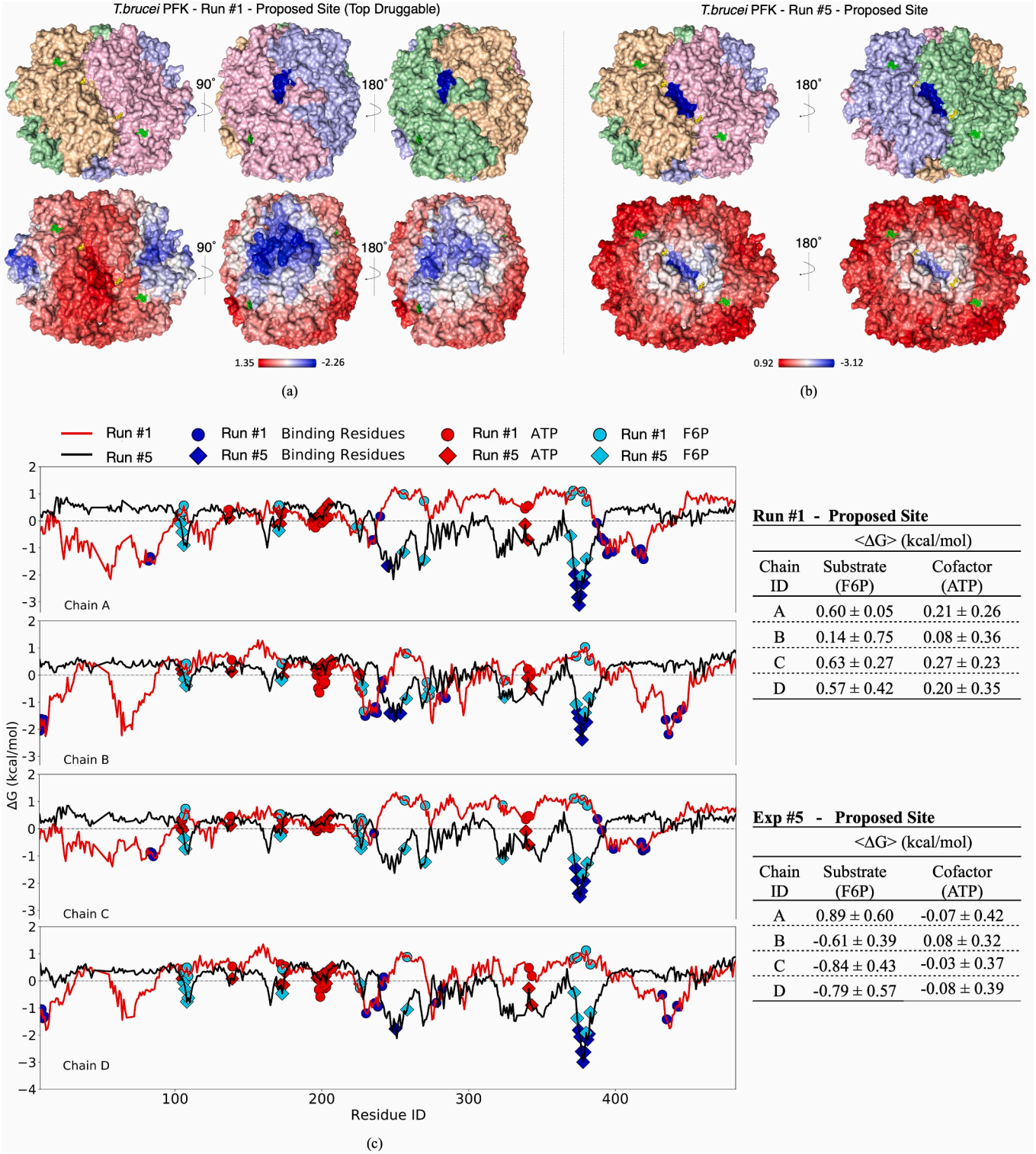

Run #1 - Proposed Site

Chain ID	<ΔG> (kcal/mol) Substrate (F6P)	Cofactor (ATP)
A	0.60 ± 0.05	0.21 ± 0.26
B	0.14 ± 0.75	0.08 ± 0.36
C	0.63 ± 0.27	0.27 ± 0.23
D	0.57 ± 0.42	0.20 ± 0.35

Exp #5 - Proposed Site

Chain ID	<ΔG> (kcal/mol) Substrate (F6P)	Cofactor (ATP)
A	0.89 ± 0.60	-0.07 ± 0.42
B	-0.61 ± 0.39	0.08 ± 0.32
C	-0.84 ± 0.43	-0.03 ± 0.37
D	-0.79 ± 0.57	-0.08 ± 0.39

Fig. 2. AlloSigMA results for *T.brucei* PFK. See caption in Fig. 1 for details.

Especially the parts where the substrate F6P would bind, displayed negative mean ΔG values as low as −0.84 kcal/mol which was the lowest observed so far. This central perturbation site was indeed critical since it also occupied the interface between two chains (A/D and its symmetric counterpart B/C), which played an essential role in regulating the global dynamics of a tetrameric complex [15,65]. Interface regions in oligomeric proteins usually accommodate "hot spot" residues, which contribute to the free energy of binding between monomeric units. Restricted dynamics imposed on these sites will eventually impact the contribution of these hot spot residues to the overall stability of the complex [66].

3.3. *No allosteric site observed in human PFK for its inhibition*

Besides bacterial/parasitic PFK, it was important to further investigate the allosteric effect in PFK of the infected human host, as the goal

was to suggest a species-specific drug molecule that would predominantly inhibit the infecting organism. As illustrated in Fig. 3, human PFK's tetrameric structure that also represented the active state, had twice the size of bacterial/parasitic PFK. It is composed of two identical dimers where each dimeric unit corresponds to one tetrameric form of bacterial/parasitic PFK. Also, each pair of chains (either A/B or C/D) in bacterial/parasitic PFK is equivalent to one monomeric unit in human PFK.

Our last analysis by Ayyildiz et al.[34] suggested a druggable site, which coincided with that of *S. aureus* PFK and *T. brucei* PFK when structurally aligned (See Figs. 1a and 2a). As the structure was composed of four identical units, the same perturbation site was selected on each of the four chains all together in the same run. The free energy of binding profile clearly indicated that all four catalytic regions displayed relatively high ΔG values, varying between 0.73 and 1.45 kcal/mol, which suggested increased dynamics (or decreased stability). Accordingly, further activation can be expected for this proposed allosteric site when occupied by any drug compound, instead of an inhibition.

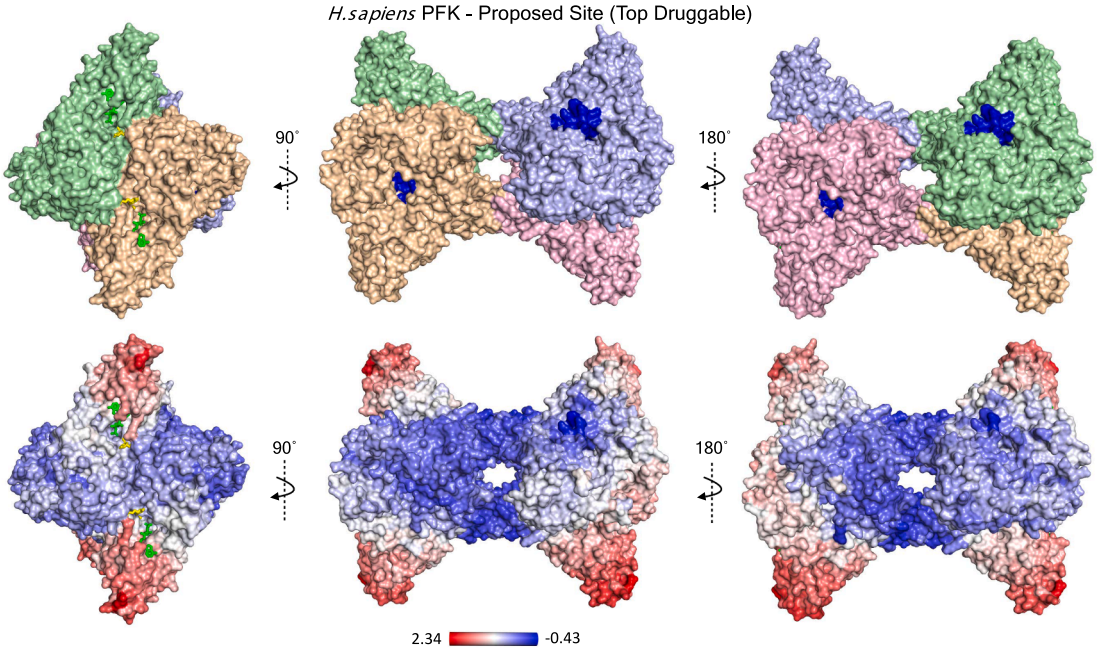

(a)

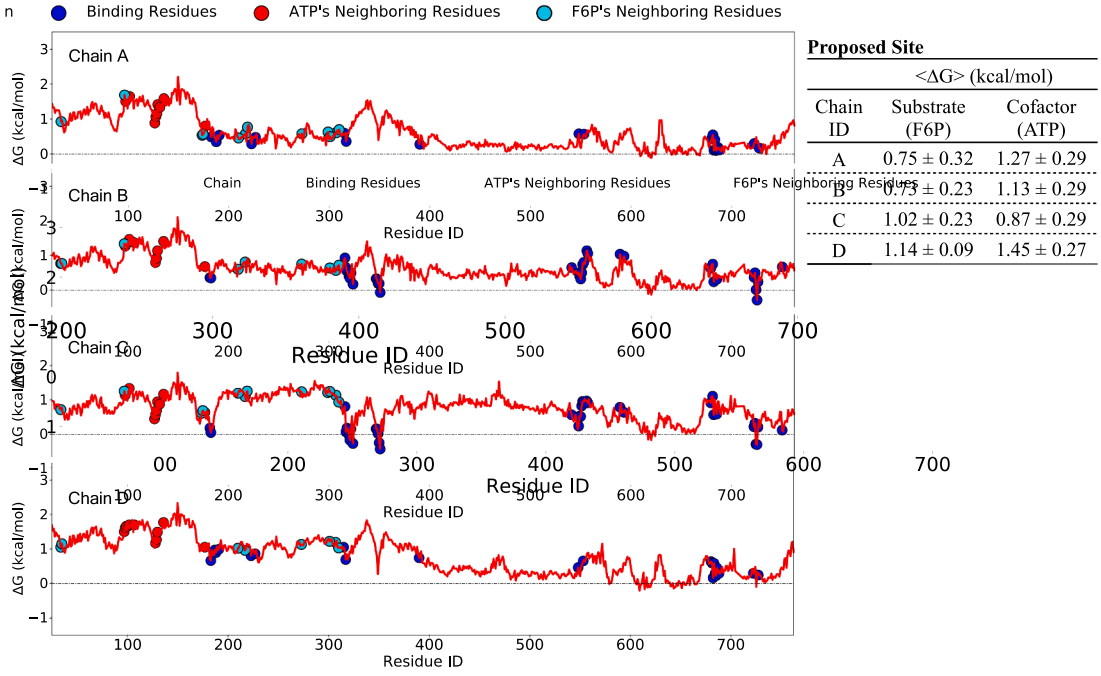

Proposed Site

Chain ID	<ΔG> (kcal/mol) Substrate (F6P)	Cofactor (ATP)
A	0.75 ± 0.32	1.27 ± 0.29
B	0.73 ± 0.23	1.13 ± 0.29
C	1.02 ± 0.23	0.87 ± 0.29
D	1.14 ± 0.09	1.45 ± 0.27

(b)

Fig. 3. AlloSigMA results for *H.sapiens* PFK. See caption in Fig. 1 for details.

3.4. Tunnel region presented itself as a novel allosteric region in Trypanosoma cruzi GADPH

In literature, no proposed allosteric site for inhibition of GADPH had been reported so far. Recently, virtual screening studies conducted by Li et al.[67] identified a novel inhibitor DC-5163, which targeted the active site directly and satisfactorily inhibited GADPH activity in five cancer cell lines. However, no information about an allosteric site that would inhibit/decrease the activity of the receptor currently exists. Our study [34] was the first to highlight the possibility of a novel allosteric site in the tunnel-like region of the receptor in either *S. aureus* or *T. cruzi*. As illustrated in the top row of Fig. 4, the central opening, which was identified as a top druggable site from our previous analysis [34], passes through the core of the receptor. It also coincides with a well-known dynamic S-shaped loop of around 20 residues, which is known to be critical for tetrameric assembly, cofactor binding and allosteric activation [68]. In a recent study by Dubey et al.[69] conducted on *T. gondii* GADPH, glycolysis in the parasite was found to be modulated by phosphorylation of the regulatory S-loop, which was a novel feature described for the first time in a species of GAPDH. Any restriction imposed on the conformational rearrangement of this tunnel-like region would directly impact the mobility of S-loop and the catalytic activity in consequence. Therefore, it was an essential target site for conducting the allostery inspection.

As illustrated in Fig. 4, the perturbation of the allosteric site in *S. aureus* PFK induced an increase of dynamics in two chains (C and D), whereas the remaining two experienced no significant change. Negative mean ΔG was observed at the binding site of substrate (G3P) and cofactor (NAD^+) of two chains A and B only. On the other hand, parasitic PFK exhibited the desired allosteric response in all four chains, especially intensified nearby substrate binding site. The same tunnel region when restricted in human PFK displayed an allosteric response similar to bacterial PFK, despite the fact that the amount of restriction at the allosteric site was comparable to that observed in parasitic PFK. Decrease in dynamics was observed in two chains' catalytic sites only. In this respect, tunnel region was clearly identified as an allosteric site for *T. cruzi* PFK that can be used for designing *T. cruzi*-specific drug molecules.

3.5. Alternative allosteric site at the large interface restricted the dynamics of all four catalytic sites in S.aureus PK

Almost a decade ago, the inhibitor IS-130 had been identified through ligand-based cheminformatics studies for methicillin-resistant *S. aureus* (*MRSA*) [50]. Following crystallographic experiments, the 3D structure of tetrameric *MRSA* PK established in complex with IS-130

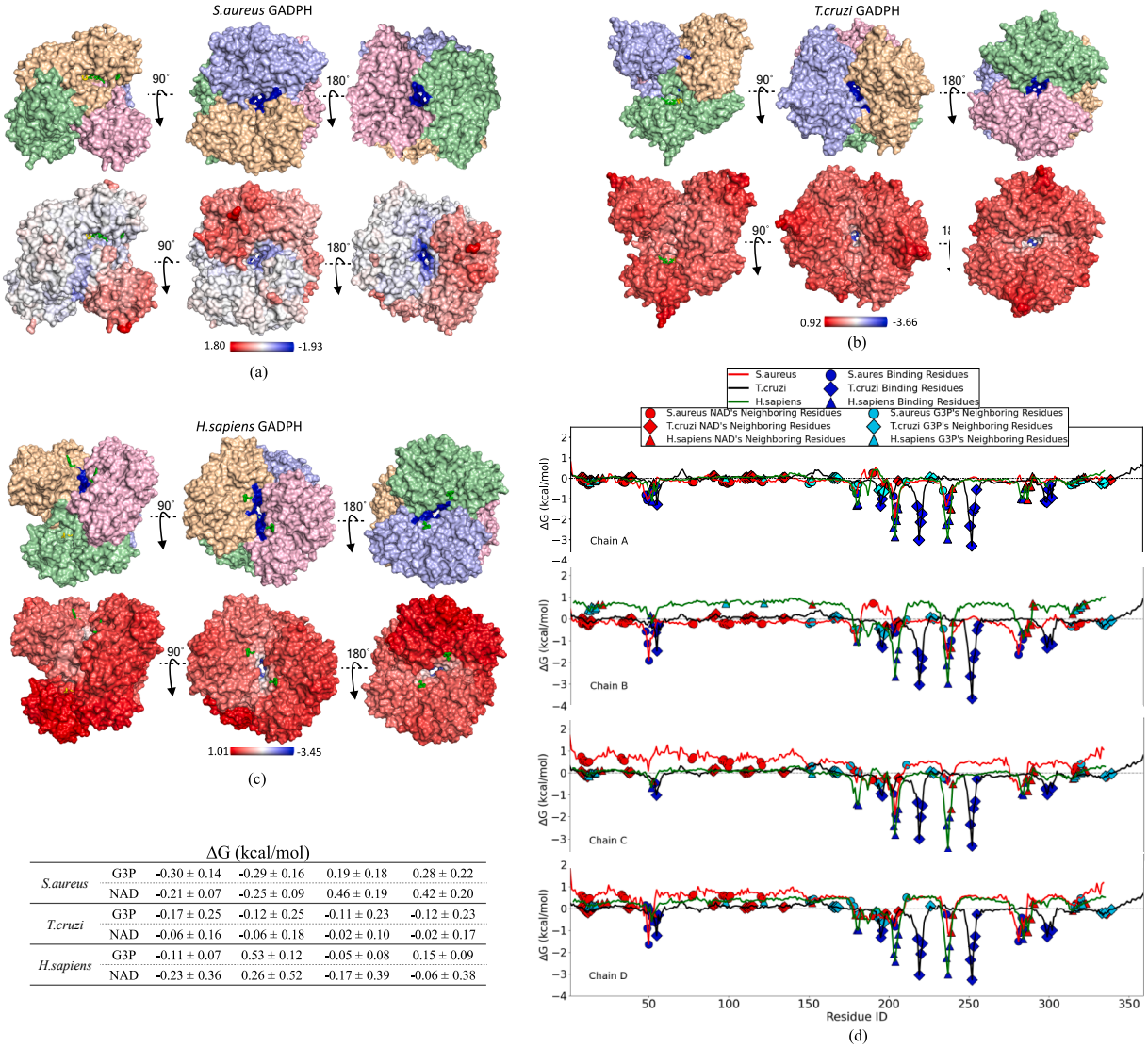

ΔG (kcal/mol)

S.aureus	G3P	-0.30 ± 0.14	-0.29 ± 0.16	0.19 ± 0.18	0.28 ± 0.22
	NAD	-0.21 ± 0.07	-0.25 ± 0.09	0.46 ± 0.19	0.42 ± 0.20
T.cruzi	G3P	-0.17 ± 0.25	-0.12 ± 0.25	-0.11 ± 0.23	-0.12 ± 0.23
	NAD	-0.06 ± 0.16	-0.06 ± 0.18	-0.02 ± 0.10	-0.02 ± 0.17
H.sapiens	G3P	-0.11 ± 0.07	0.53 ± 0.12	-0.05 ± 0.08	0.15 ± 0.09
	NAD	-0.23 ± 0.36	0.26 ± 0.52	-0.17 ± 0.39	-0.06 ± 0.38

Fig. 4. AlloSigMA results for GADPH of all three species (a) *S. aureus*, (b) *T. cruzi* and (c) *H. sapiens*. See caption in Fig. 1.

(PDB id: 3t0t) revealed that the inhibitor bound to the C-domain interface prevented the salt bridges between C—C small interface, which were critical for the transition to the active state [54]. In this study, an alternative druggable site recognized from our last study [34] located at the so-called large A-domain interface (See Fig. 5a) was used in AlloSigMA trials. Similar to the known allosteric site, this alternative spot also had a symmetric counterpart across the other side of the central opening. Allostery evaluations were conducted both on the alternative proposed sites and the known sites for comparison. As indicated in Fig. 6a, the restriction of the proposed site allosterically decreased the dynamics of all four catalytic regions with mean ΔG between −0.33 and − 0.01 kcal/mol, whereas a similar restriction imposed on the known allosteric site triggered an increase in the dynamics of all four catalytic regions represented by a mean ΔG between 0.06 and 0.18 kcal/mol.

3.6. Partial inhibition in H. sapiens and L. mexicana PK

Our previous analysis highlighted a druggable site in L. *mexicana* PK in one chain only, as depicted in Fig. 5b. This site also existed in bacterial (*S. aureus*) PK, however it was overlooked for this study, as it didn't rank in the highest score list. The allosteric effect of this region on three out of four catalytic sites was satisfactory, i.e., it had the inhibition feature recognized by negative mean values of free energy of binding. The fourth catalytic site displayed no effect with negligibly small positive mean ΔG between 0.01 and 0.08 kcal/mol (See Fig. 6b.). Satisfactory results were observed in human PK for the proposed allosteric site which coincided with the same location at the large interface as in bacterial PK. Yet, as illustrated in Fig. 6c, the conformational rearrangement in human PK almost completely closed the central opening. Restricted

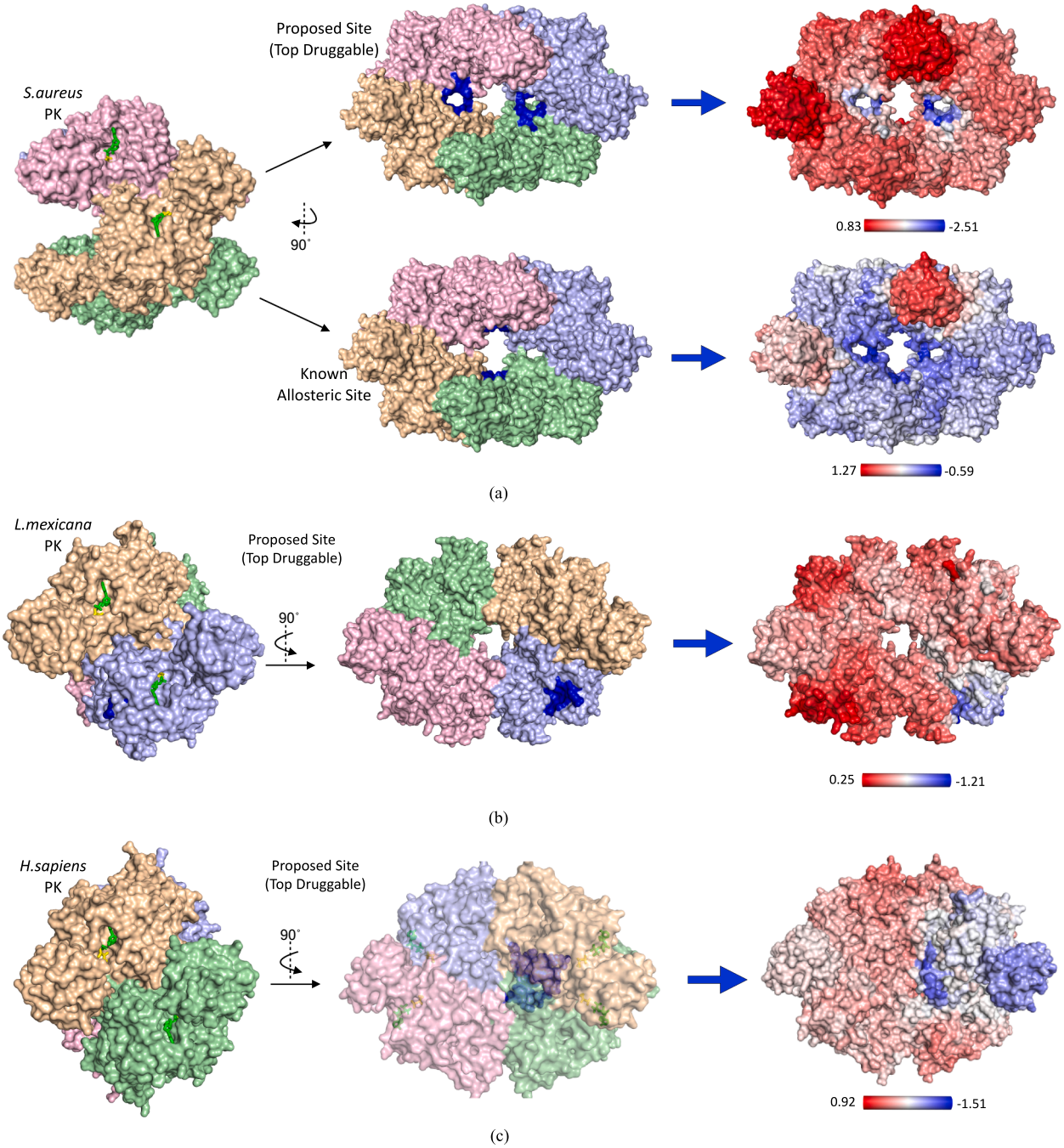

Fig. 5. Perturbation sites in PK of all three species, (a) *S. aureus*, (b) *L. mexicana* and (c) *H. sapiens* and their corresponding AlloSigMA results.

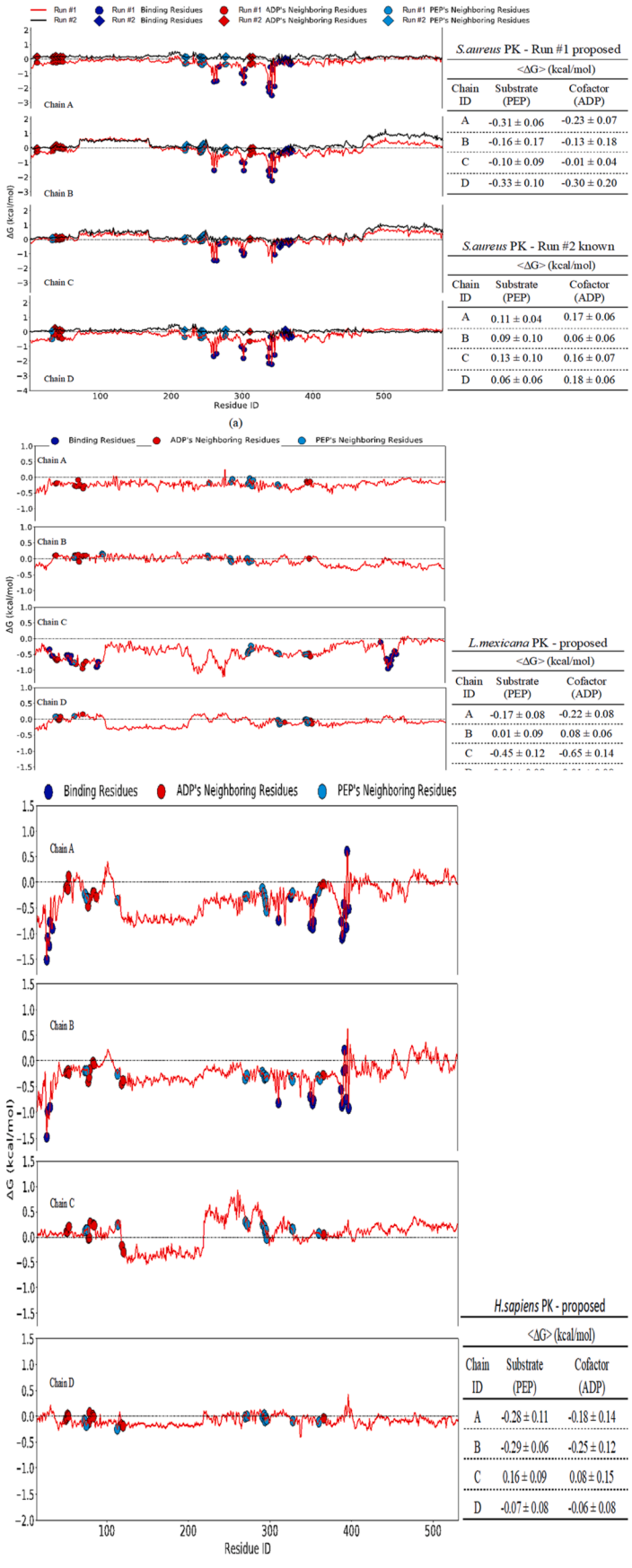

Fig. 6. Profiles for free energy of binding for (a) *S. aureus* PK (b) *L. mexicana* PK and (c) *H. sapiens* PK enzymes with corresponding mean ΔG values at the substrate (PEP) and cofactor (ADP) binding site.

dynamics observed in the other three catalytic sites except chain C, clearly emphasized the likelihood of this site to be allosteric, yet not as strongly as in *S. aureus* PK.

3.7. Proposed allosteric sites accommodated hub residues in all three receptors

The residue network model examined the contact topology of the investigated glycolytic enzymes and suggested residues with a high potential to take part on the communication pathways between distant regions of the structure, such as allosteric and active sites. These so-called hub residues presumably transmit a perturbation due to ligand binding through tertiary interactions and conformational changes [37]. The method was applied to multiple X-ray crystallographic structures of the receptor which also represented multiple conformations, in order to improve the sampling of the residue contacts.

For each enzyme, a total of 12–13 X-ray crystal structures was used for all three species, *H.sapiens*, *S.aureus* and *T. brucei* (See Table 1 for PDB ids). Hub residues of the network with highest betweenness values in the top 5% were determined and listed in supplementary Tables S5 through S7. Furthermore, hub residues located at either proposed or known allosteric sites were extracted and highlighted as in Fig. 7 and also listed in Table 3. For *S. aureus* PFK, a total of 24 hub residues (6 per chain) were detected at the proposed site whereas 12 hub residues (3 per chain) were observed at the known allosteric site. Similarly, a considerable amount of hub residues (a total of 20) were detected at five different proposed allosteric sites and their nearest neighbours in *T. brucei* PFK, as listed in Table 3 and Table S5. Moreover, human PK incorporated several hub residues at the proposed allosteric site; R683, N684, F685 on chains A and D, and A316, R324, N541, S549, N557, and F685 on chains B and C which amount to 28 hub residues in total.

Hub residues traced plausible allosteric communication pathways between distant functional sites and for PFK enzyme; they were mostly concentrated at the dimeric and tetrameric interfaces. For example in *H. sapiens* PFK, S84 and I85 take an essential part in the dimerization interface of chains B and D. The allosteric activator FBP binds to E639, R576, R665, and R744, which are next to the dimer interface [42]. Conserved residue S540 that blocks the PFK glycosylation and thus impairing cancer cell proliferation also had high betweenness score. For

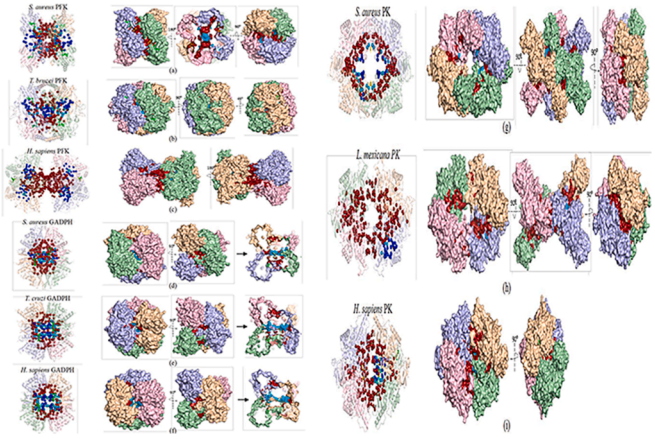

Fig. 7. Residues with high betweenness scores (hub) residues in PFK, GADPH and PK for three different species (a), (d), (g) *S.aureus* (b), (e), (h) *T. brucei* and (c), (f), (i) *H. sapiens,* respectively. Hub residues at either proposed or known allosteric sites (See Table 3) represented in cyan. Dark blue spheres correspond to residues at the proposed sites calculated by AlloSigMA. ATP (green), F6P (yellow) explicitly shown in (a). DZG, substrate of *H. sapiens* PK (PDB: 3gqy) and IS-130, the known inhibitor of *S.aureus* PK indicated in yellow in each structure in (g), (i). (chain A: wheat, chain B: pale green, chain C: light blue, chain D: light pink). (For interpretation of the references to colour in this figure legend, the reader is referred to the web version of this article.)

Table 3
Hub residues located at the allosteric sites in all three species of all three enzymes.

Enzyme	Species	Trial Runs	Hub Residues (Chain ID: Residue IDs)	TOTAL # of hub residues
PFK	*S.aureus*	#1 Proposed Site (Top Druggable)	**A:** G140, N146, T259, G260, D262, V264 **B:** G140, N146, T259, G260, D262, V264 **C:** G140, N146, T259, G260, D262, V264 **D:** G140, N146, T259, G260, D262, V264	24
		#2 Known Allosteric Site	**A:** R156, V186, E189 **B:** R156, V186, E189 **C:** R156, V186, E189 **D:** R156, V186, E189	12
	T.brucei	#1 Proposed Site (Top Druggable)	**A:** R237, Q242, N390, L398 **B:** N230, H236, R237, T238, F241, Q242 **C:** R237, Q390 **D:** N230, H236, F241, Q242	16
		#5 Proposed Site	**A:** A254, Y380, I382 **B:** A254, Y380 **C:** Y380 **D:** Y380, I382	8
	H.Sapiens	Proposed Site (Top Druggable)	**A:** R683-F685 **B:** A316, R324, N541, S549, N557, F685 **C:** A316, R324, N541, S549, N557, F685 **D:** R683-F685	18
GADPH	*S.aureus*	Proposed Site	**A:** T49, E204, N205, P236-A238 **B:** T49, E204, N205, P236, A238, T239, S281, D282 **C:** E204, P236 **D:** T49, E204, P236, S281-V283	22
	T.cruzi	Proposed Site	**A:** T54, V55, I221, P251-V255, S298, A299, I302 **B:** T54-H56, R212, P251-S256, S298, A299, I302 **C:** T54, V55, I221, P251-V255, S298, A299, I302 **D:** T54-H56, I221, P251-V255, S298, A299, I302	47
	H.Sapiens	Proposed Site (Top Druggable)	**A:** T52, H53, I206, P236, A238-V240, S283, S284, N287 **B:** S51, T52, I206, P236, A238-V240, S283, S284, N287 **C:** S51, T52, I206, P236, A238-V240, S283, S284, N287 **D:** S51, T52, I206, P236, A238-V240, S283, S284, N287, D288	41
PK	*S.aureus*	#1 Proposed Site (Top Druggable)	**A:** N267, N299, D303 G304, A337, Q338 **B:** N299, D303, A337, Q338 **C:** N267, K268, N299, D303 **D:** Q338	15
			A: I361, S362 **B:** I361, S362	8

(*continued on next page*)

Table 3 (*continued*)

Enzyme	Species	Trial Runs	Hub Residues (Chain ID: Residue IDs)	TOTAL # of hub residues
		#2 Known Allosteric Site	**C:** I361, S362 **D:** I361, S362	
		#3 Proposed Site	**A:** K271 **B:** G483, R484	3
	L. mexicana	Proposed Site (Top Druggable)	**C:** R19, C420, I433, T434	4
	H.Sapiens	Proposed Site (Top Druggable)	**A:** F26, H29, M30, L33, N350, V352, A388-H391, E397 **B:** F26, M30, N350, A388-L392, E397	20

S.aureus PFK, there exist several hub residues such as G126-I128, M171, G172, H251, R254 [38] establishing hydrogen bonding and secondary non-covalent interactions with F6P. Moreover, two hub residues R164 and R245 maintain the tetramer stability. Similarly, hub residues in *T. brucei*, were concentrated on the tetrameric interfaces, and also A/D, B/C chain interfaces. Two hub residues N230 and G273 neighboring the catalytic site residue D229, and ATP binding residues G107 and K226 [39] were detected in the analysis.

The second allosteric enzyme GAPDH was similarly explored for hub residues using a total of 13 X-ray crystal structures belonging to three different species; 4 for *H.sapiens,* 5 for *S.aureus* and 4 for *T.cruzi* (See Table 1). Hub residues were then illustrated on the structure of GAPDH as in Fig. 7d, e, f. The complete list of hub residues was given in Table S6. Residue network model clearly supported our proposed allosteric site predictions pointing to the tunnel-like region of GAPDH which incorporated several hub residues in all three species; 22 for *S. aureus*, 47 for *Trigonoscuta cruzi*, and 41 for *H. sapiens* (See Table 3).

Moreover, our network model successfully captured critical regions in all three species of GAPDH as hubs and pointed to possible communication pathways in the structure. For instance, in *S. aureus PFK*, the catalytic residue H178, the S-loop (residues 179–206) in the catalytic domain, the phosphate recognition site S150, T211, H178, R234, the 209–215 loop, and glyceraldehyde 3-phosphate binding R234 [43] were all detected as hub residues by the residue network model. Similarly, for *T. cruzi*, R12 residue interacting with NAD [46], glyceraldehyde 3-phosphate binding residue R249, and H194 critical in catalytic activity had been captured as hub residues. Finally, in *H. sapiens GADPH,* H179 activating thiol during catalysis, nucleotide-binding residues R13, and its neighbour F11, the catalytic residue C152 were determined as hub residues with the highest betweenness values.[50]

Finally, the hub residues were revealed for the allosteric PK enzyme as illustrated in Fig. 7g, h, i and listed in Table S7. For *S. aureus* PK, the amount of hub residues accommodated at the proposed allosteric site (top druggable) located at the central region was twice as much as that observed at the known allosteric site, whereas the second proposed allosteric site (Run #3) had the least amount of hub residues. For L. *mexicana* PK, four residues R19, C420, I433, and T434 displayed high betweenness scores at the proposed top druggable allosteric site. Finally, *H. sapiens PK* included the highest number of hub residues at the proposed allosteric site, which is 20. Other hub residues coincided with amino acids of functional importance, such as ATP binding residues R120 and K207 and substrate binding residue G295 [57], as well as K305 and E384 related with inactivation of PK in human [70]. In *S. aureus*, substrate-binding residues *G244 and T277, inhibitor IS-130 binding residues I361 and S362 at the dimer interface were also revealed as hub residues. In* L. *mexicana PK, the active site residues R262 and G266, and the salt bridge interaction pair* D482 and R493 at *C*—C interface [56] important for allosteric regulation were captured by the residue network model as hub residues.

4. Concluding remarks

Two different theoretical approaches were employed to strengthen the likelihood of previously proposed binding sites to hold the desired allosteric effect; deformation of low-frequency normal modes that describe the global dynamics and the centrality measure of betweenness based solely on contact topology. Both techniques used a simplified network model of C_α atoms only. First technique provides a change in the free energy as a result of perturbation (or ligand binding) which is defined in terms of low-frequency normal modes. A negative value indicates a stabilization in the corresponding region, whereas a positive value represents a destabilization caused by allosteric binding. Three different glycolytic enzymes from three different species (bacterial, parasitic and human) were under investigation separately. The purpose of including the human species was to identify allosteric sites which would display a high degree of sequence variation among species and consequently, would be an ideal target site for the design of species-specific drugs. For this study, it enabled us to compare the degree of allosteric effect of selected regions for the same enzyme in different species.

For *S. aureus* bacterial PFK enzyme, an experimentally reported allosteric site was used for comparison with the proposed one. Accordingly, stabilization indicated by a negative mean free energy value ($<\Delta G>$) was observed in the dynamics of all four catalytic regions of the homotetramer in the range of −0.78 and − 0.18 kcal/mol, when the proposed site was perturbed. On the other hand, there was no significant change in the dynamics of the same regions when the known allosteric site was used for perturbation. Another PFK enzyme investigated for allostery belonged to *T. brucei* parasitic species. First evaluation was conducted on a top druggable site which also coincided with that of bacteria. However, the range of $<\Delta G>$ values was 0.08–0.63 kcal/mol which reflected a destabilization of the dynamics in the catalytic regions. Four more perturbation sites were then selected and the last trial run which targeted an interface region between two chains induced a noticeable restriction in the dynamics of the catalytic regions. The fact that this target region was found at the interface further enhanced its likelihood to be allosteric as interfaces accommodated “hot spot” residues, which contributed to the free energy of binding between monomeric units and hence the global dynamics. Finally, for *H. sapiens* PFK, an allosteric activation was observed for the selected proposed sites, instead of an inhibition.

A tunnel region passing through the core of the receptor was identified for allosteric inhibition in GADPH. Trial runs were conducted for all three species, *S. aureus*, *T. cruzi* and *H. sapiens* on the same tunnel as the perturbation site. Accordingly, the strongest allosteric inhibition effect was observed for *T. cruzi* parasitic GAPDH where the restriction of the dynamics was observed in all four catalytic regions with negative $<\Delta G>$ values, whereas a partial inhibition was detected in two out of four catalytic regions for both bacterial and human GAPDH. Accordingly, tunnel region was proposed as a target spot for the discovery of *T. cruzi*-specific drug molecules.

Similar to PFK enzyme, an experimentally identified allosteric region at the small C-domain interface of PK enzyme where the allosteric inhibitor IS-130 was observed in the resolved crystallographic structure was used for comparison with the proposed allosteric site which was located at the large A-domain interface. The location of both sites was nearby the central opening. Upon perturbation, the proposed site clearly outperformed the known allosteric one, by restricting the dynamics of all four catalytic regions, where an increase in the dynamics was observed when the known allosteric site was perturbed. For parasitic PK, an allosteric site which was further away from the central opening was suggested. However, only a partial inhibition was observed, with $<\Delta G>$ values noticeably negative in two chains only. In human PK, the corresponding A-domain interface at the central region was also suggested as a proposed allosteric site. However, in human PK, the centre was completely closed in a distinct conformational rearrangement. Similar to

parasitic PK, a partial restriction in global dynamics was observed, i.e., only two chains displayed noticeable negative <ΔG> values.

In the second part of the study, the centrality measure of betweenness based solely on contact topology was employed on three enzymes of three species. The goal was to identify the hub residues that were suggested to take part on the communication pathways between distant sites, and indetify those that were located at the suggested proposed regions to strengthen the likelihood of their allosteric features. Accordingly, a significant portion of the hub residues were accommodated in either proposed or known allosteric regions. Especially, it was promising to observe twice as many hub residues at the proposed sites as those at the known sites for bacterial PFK and bacterial PK enzymes. Moreover, the strongest allosteric effect observed for the tunnel region of parasitic GADPH also incorporated the highest number of hub residues observed in any of the studied systems. Also, there exists a direct correspondence between the degree of allosteric effect of a site and the number of hub residues it incorporates for the majority of the systems. The number of hub residues among bacterial and human PK were comparable and located at the centre. However, there was a major structural divergence in *H. sapiens* PK which presented a closed centre as opposed to an open one recognized in *S. aureus* PK. Hence, this structural difference between human and bacterial PKs was proposed as an ideal target site for the design of species-specific drugs which will bind more strongly to bacterial PK than its human counterpart.

Author contributions

The manuscript was written through the contributions of all authors. All authors have given approval to the final version of the manuscript.

Declaration of competing interest

The authors have no conflict of interest to declare.

Data availability

Data will be made available on request.

Acknowledgment

This work has been partially supported by The Scientific and Technological Research Council of Turkey (TÜBİTAK Project # 218 M320).

Appendix A. Supplementary data

Supplementary data to this article can be found online at https://doi.org/10.1016/j.bpc.2021.106701.

References

[1] K. Gunasekaran, B. Ma, R. Nussinov, Is allostery an intrinsic property of all dynamic proteins? Proteins. 57 (3) (2004) 433–443.
[2] E.W. Yu, D.E. Koshland Jr., Propagating conformational changes over long (and short) distances in proteins, Proc. Natl. Acad. Sci. U. S. A. 98 (17) (2001) 9517–9520.
[3] J. Monod, J. Wyman, J.-P. Changeux, On the nature of allosteric transitions: a plausible model, J. Mol. Biol. 12 (1) (1965) 88–118.
[4] D.E. Koshland Jr., G. Némethy, D. Filmer, Comparison of experimental binding data and theoretical models in proteins containing subunits, Biochemistry. 5 (1) (1966) 365–385.
[5] W.A. Lim, The modular logic of signaling proteins: building allosteric switches from simple binding domains, Curr. Opin. Struct. Biol. 12 (1) (2002) 61–68.
[6] C.M. Falcon, K.S. Matthews, Engineered disulfide linking the hinge regions within lactose repressor dimer increases operator affinity, decreases sequence selectivity, and alters allostery, Biochemistry. 40 (51) (2001) 15650–15659.
[7] X. Wang, R.G. Kemp, Reaction path of phosphofructo-1-kinase is altered by mutagenesis and alternative substrates, Biochemistry. 40 (13) (2001) 3938–3942.
[8] B. Santamaria, A.M. Estevez, O.H. Martinez-Costa, J.J. Aragon, Creation of an allosteric phosphofructokinase starting with a nonallosteric enzyme. The case of dictyostelium discoideum phosphofructokinase, J Biol Chem. 277 (2) (2002) 1210–1216.
[9] C. Pargellis, L. Tong, L. Churchill, et al., Inhibition of p38 MAP kinase by utilizing a novel allosteric binding site, Nat. Struct. Biol. 9 (4) (2002) 268–272.
[10] W.V. Tee, E. Guarnera, I.N. Berezovsky, Reversing allosteric communication: from detecting allosteric sites to inducing and tuning targeted allosteric response, PLOS Comp Biol. 14 (6) (2018), e1006228.
[11] J. Ellis, Allosteric binding sites on muscarinic receptors, Drug Dev. Res. 40 (4) (1997) 349.
[12] A. Christopoulos, Allosteric binding sites on cell-surface receptors: novel targets for drug discovery, Nat. Rev. Drug Discov. 1 (3) (2002) 198–210.
[13] N.A. Temiz, I. Bahar, Inhibitor binding alters the directions of domain motions in HIV-1 reverse transcriptase, Proteins. 49 (1) (2002) 61–70.
[14] S. Piana, P. Carloni, M. Parrinello, Role of conformational fluctuations in the enzymatic reaction of HIV-1 protease, J. Mol. Biol. 319 (2) (2002) 567–583.
[15] S. Mitternacht, I.N. Berezovsky, Binding leverage as a molecular basis for allosteric regulation, PLoS Comput. Biol. 7 (9) (2011), e1002148.
[16] Z. Kurkcuoglu, D. Findik, E.D. Akten, P. Doruker, How an inhibitor bound to subunit interface alters triosephosphate isomerase dynamics, Biophys. J. 109 (6) (2015) 1169–1178.
[17] M.A. Young, S. Gonfloni, G. Superti-Furga, B. Roux, J. Kuriyan, Dynamic coupling between the SH2 and SH3 domains of c-Src and Hck underlies their inactivation by C-terminal tyrosine phosphorylation, Cell. 105 (1) (2001) 115–126.
[18] D.E. Koshland Jr., Conformational changes: how small is big enough? Nat. Med. 4 (10) (1998) 1112–1114.
[19] A. Cooper, D.T.F. Dryden, Allostery without conformational change, Eur. Biophys. J. 11 (1984) 103–109.
[20] J.-P. Changeux, S.J. Edelstein, Allosteric mechanisms of signal transduction, Science. 308 (5727) (2005) 1424–1428.
[21] D. Bray, T. Duke, Conformational spread: the propagation of allosteric states in large multiprotein complexes, Annu. Rev. Biophys. Biomol. Struct. 33 (1) (2004) 53–73.
[22] R.O. Hynes, Integrins: bidirectional, allosteric signaling machines, Cell. 110 (6) (2002) 673–687.
[23] R.D. Vale, R.A. Milligan, The way things move: looking under the hood of molecular motor proteins, Science. 288 (5463) (2000) 88–95.
[24] A. del Sol, C.-J. Tsai, B. Ma, R. Nussinov, The origin of allosteric functional modulation: multiple pre-existing pathways, Structure. 17 (8) (2009) 1042–1050.
[25] D. Datta, J.M. Scheer, M.J. Romanowski, J.A. Wells, An allosteric circuit in caspase-1, J. Mol. Biol. 381 (5) (2008) 1157–1167.
[26] C. Chennubhotla, I. Bahar, Markov propagation of allosteric effects in biomolecular systems: application to GroEL-GroES, Mol. Syst. Biol. 2 (1) (2006) 36.
[27] L.H. Greene, V.A. Higman, Uncovering network systems within protein structures, J. Mol. Biol. 334 (4) (2003) 781–791.
[28] H. Jeong, S.P. Mason, A.L. Barabási, Z.N. Oltvai, Lethality and centrality in protein networks, Nature. 411 (6833) (2001) 41–42.
[29] A. del Sol, H. Fujihashi, D. Amoros, R. Nussinov, Residues crucial for maintaining short paths in network communication mediate signaling in proteins, Mol. Syst. Biol. 2 (1) (2006) 2006.0019.
[30] J.J. Perona, L. Hedstrom, W.J. Rutter, R.J. Fletterick, Structural origins of substrate discrimination in trypsin and chymotrypsin, Biochemistry. 34 (5) (1995) 1489–1499.
[31] E. Guarnera, I.N. Berezovsky, Allosteric drugs and mutations: chances, challenges, and necessity, Curr. Opin. Struct. Biol. 62 (2020) 149–157.
[32] E. Guarnera, I.N. Berezovsky, Toward comprehensive allosteric control over protein activity, Structure. 27 (2019) 866–878.
[33] R. Nussinov, C.J. Tsai, Allostery in disease and in drug discovery, Cell. 153 (2013) 293–305.
[34] M. Ayyildiz, S. Celiker, F. Ozhelvaci, E.D. Akten, Identification of alternative allosteric sites in glycolytic enzymes for potential use as species-specific drug targets, Front. Mol. Biosci. 7 (2020) 88.
[35] E. Guarnera, I.N. Berezovsky, Structure-based statistical mechanical model accounts for the causality and energetics of allosteric communication, PLoS Comput. Biol. 12 (3) (2016), e1004678.
[36] E. Guarnera, Z.W. Tan, Z. Zheng, I.N. Berezovsky, AlloSigMA: allosteric signaling and mutation analysis server, Bioinformatics. 33 (24) (2017) 3996–3998.
[37] E. Guarnera, I.N. Berezovsky, On the perturbation nature of allostery: sites, mutations, and signal modulation, Curr. Opin. Struct. Biol. 56 (2019) 18–27.
[38] O. Kurkcuoglu, Exploring allosteric communication in multiple states of the bacterial ribosome using residue network analysis, Turk. J. Biol. 42 (5) (2018) 392–404.
[39] T. Tian, C. Wang, M. Wu, X. Zhang, J. Zang, Structural insights into the regulation of staphylococcus aureus phosphofructokinase by tetramer–dimer conversion, Biochemistry. 57 (29) (2018) 4252–4262.
[40] I.W. McNae, J. Martinez-Oyanedel, J.W. Keillor, P.A.M. Michels, L.A. Fothergill-Gilmore, M.D. Walkinshaw, The crystal structure of ATP-bound phosphofructokinase from Trypanosoma brucei reveals conformational transitions different from those of other phosphofructokinases, J. Mol. Biol. 385 (5) (2009) 1519–1533.
[41] J. Martinez-Oyanedel, I.W. McNae, M.W. Nowicki, et al., The first crystal structure of phosphofructokinase from a eukaryote: Trypanosoma brucei, J. Mol. Biol. 366 (4) (2007) 1185–1198.
[42] I.W. McNae, J. Kinkead, D. Malik, et al., Fast acting allosteric phosphofructokinase inhibitors block trypanosome glycolysis and cure acute African trypanosomiasis in mice, Nat. Commun. 12 (1) (2021) 1052.
[43] M. Kloos, A. Brüser, J. Kirchberger, T. Schöneberg, N. Sträter, Crystal structure of human platelet phosphofructokinase-1 locked in an activated conformation, Biochem. J. 469 (3) (2015) 421–432.

[44] S. Mukherjee, D. Dutta, B. Saha, A.K. Das, Crystal structure of glyceraldehyde-3-phosphate dehydrogenase 1 from methicillin-resistant Staphylococcus aureus MRSA252 provides novel insights into substrate binding and catalytic mechanism, J. Mol. Biol. 401 (5) (2010) 949–968.
[45] R. Guido, T. Balliano, A. Andricopulo, G. Oliva, Kinetic and crystallographic studies on glyceraldehyde-3-phosphate dehydrogenase from Trypanosoma cruzi in complex with iodoacetate, Lett Drug Des Discov. 6 (3) (2009) 210–214.
[46] F. Pavão, M.S. Castilho, M.T. Pupo, et al., Structure ofTrypanosoma cruziglycosomal glyceraldehyde-3-phosphate dehydrogenase complexed with chalepin, a natural product inhibitor, at 1.95 Å resolution, FEBS Lett. 520 (1–3) (2002) 13–17.
[47] M.S. Castilho, F. Pavão, G. Oliva, S. Ladame, M. Willson, J. Périé, Evidence for the two phosphate binding sites of an analogue of the thioacyl intermediate for the Trypanosoma cruzi glyceraldehyde-3-phosphate dehydrogenase-catalyzed reaction, from its crystal structure, Biochemistry. 42 (23) (2003) 7143–7151.
[48] S. Ladame, M.S. Castilho, C.H.T.P. Silva, et al., Crystal structure of Trypanosoma cruzi glyceraldehyde-3-phosphate dehydrogenase complexed with an analogue of 1,3-bisphospho-d-glyceric acid. Selective inhibition by structure-based design, Eur. J. Biochem. 270 (22) (2003) 4574–4586.
[49] M.R. White, M.M. Khan, D. Deredge, et al., A dimer interface mutation in glyceraldehyde-3-phosphate dehydrogenase regulates its binding to AU-rich RNA, J. Biol. Chem. 290 (3) (2015) 1770–1785.
[50] J.B. Park, H. Park, J. Son, S.-J. Ha, H.-S. Cho, Structural study of monomethyl fumarate-bound human GAPDH, Mol Cells. 42 (8) (2019) 597–603.
[51] P. Axerio-Cilies, R.H. See, R. Zoraghi, et al., Cheminformatics-driven discovery of selective, nanomolar inhibitors for staphylococcal pyruvate kinase, ACS Chem. Biol. 7 (2) (2012) 350–359.
[52] R. Zoraghi, L. Worrall, R.H. See, et al., Methicillin-resistant Staphylococcus aureus (MRSA) pyruvate kinase as a target for bis-indole alkaloids with antibacterial activities, J. Biol. Chem. 286 (52) (2011) 44716–44725.
[53] D.J. Rigden, S.E. Phillips, P.A. Michels, L.A. Fothergill-Gilmore, The structure of pyruvate kinase from Leishmania mexicana reveals details of the allosteric transition and unusual effector specificity, J. Mol. Biol. 291 (3) (1999) 615–635.
[54] L.B. Tulloch, H.P. Morgan, V. Hannaert, P.A.M. Michels, L.A. Fothergill-Gilmore, M.D. Walkinshaw, Sulphate removal induces a major conformational change in Leishmania mexicana pyruvate kinase in the crystalline state, J. Mol. Biol. 383 (3) (2008) 615–626.
[55] H.P. Morgan, I.W. McNae, M.W. Nowicki, et al., Allosteric mechanism of pyruvate kinase from Leishmania mexicana uses a rock and lock model, J. Biol. Chem. 285 (17) (2010) 12892–12898.
[56] C. Kung, J. Hixon, S. Choe, et al., Small molecule activation of PKM2 in cancer cells induces serine auxotrophy, Chem. Biol. 19 (9) (2012) 1187–1198.
[57] J.D. Dombrauckas, B.D. Santarsiero, A.D. Mesecar, Structural basis for tumor pyruvate kinase M2 allosteric regulation and catalysis, Biochemistry. 44 (27) (2005) 9417–9429.
[58] H.P. Morgan, F.J. O'Reilly, M.A. Wear, et al., M2 pyruvate kinase provides a mechanism for nutrient sensing and regulation of cell proliferation, Proc. Natl. Acad. Sci. U. S. A. 110 (15) (2013) 5881–5886.
[59] M. Yuan, I.W. McNae, Y. Chen, et al., An allostatic mechanism for M2 pyruvate kinase as an amino-acid sensor, Biochem. J. 475 (10) (2018) 1821–1837.
[60] R. Brenke, D. Kozakov, G.Y. Chuang, D. Beglov, D. Hall, M.R. Landon, C. Mattos, S. Vajda, Fragment-based identification of druggable 'hot spots' of proteins using fourier domain correlation techniques, Bioinformatics. 25 (2009) 621–627.
[61] B.T. Kaynak, D. Findik, P. Doruker, RESPEC incorporates residue specificity and the ligand effect into the elastic network model, J. Phys. Chem. B 122 (2018) 5347–5355.
[62] T. Schirmer, P.R. Evans, Structural basis of the allosteric behaviour of phosphofructokinase, Nature. 343 (6254) (1990) 140–145.
[63] V. Saraswathi, A network representation of protein structures: implications for protein stability, Biophys. J. 89 (6) (2005) 4159–4170.
[64] O. Kurkcuoglu, O.T. Turgut, S. Cansu, R.L. Jernigan, P. Doruker, Focused functional dynamics of supramolecules by use of a mixed-resolution elastic network model, Biophys. J. 97 (4) (2009) 1178–1187.
[65] Z. Kurkcuoglu, G. Ural, E.D. Akten, P. Doruker, Blind dockings of benzothiazoles to multiple receptor conformations of triosephosphate isomerase from Trypanosoma cruzi and human, Mol Inform. 30 (11−12) (2011) 986–995.
[66] A.A. Bogan, K.S. Thorn, Anatomy of hot spots in protein interfaces, J. Mol. Biol. 280 (1) (1998) 1–9.
[67] T. Li, X. Tan, R. Yang, et al., Discovery of novel glyceraldehyde-3-phosphate dehydrogenase inhibitor via docking-based virtual screening, Bioorg. Chem. 96 (103620) (2020) 103620.
[68] G. Biesecker, J.I. Harris, J.C. Thierry, J.E. Walker, A.J. Wonacott, Sequence and structure of D-glyceraldehyde 3-phosphate dehydrogenase from Bacillus stearothermophilus, Nature. 266 (5600) (1977) 328–333.
[69] R. Dubey, B.L. Staker, I.T. Foe, et al., Membrane skeletal association and post-translational allosteric regulation of toxoplasma gondii GAPDH1, Mol. Microbiol. 103 (4) (2017) 618–634.
[70] D. Anastasiou, Y. Yu, W.J. Israelsen, et al., Pyruvate kinase M2 activators promote tetramer formation and suppress tumorigenesis, Nat. Chem. Biol. 8 (10) (2012) 839–847.